Monthly Notices of the ROYAL ASTRONOMICAL SOCIETY

MNRAS **546,** 1–11 (2026) https://doi.org/10.1093/mnras/staf2224
Advance Access publication 2025 December 19

Laboratory rotational spectroscopy and interstellar search for the protein precursor 4-oxobutanenitrile ($HCOCH_2CH_2CN$)

V. M. Rivilla [1★†] E. R. Alonso,[2,3†‡] W. Song,[4†] A. Insausti,[2,3] A. Maris [4,5] F. J. Basterretxea,[2] S. Melandri [4,5★] I. Jiménez-Serra[1] and E. J. Cocinero [2,3★]

[1]*Centro de Astrobiología (CAB, CSIC-INTA), Ctra. de Ajalvir Km. 4, Torrejón de Ardoz, E-28850 Madrid, Spain*
[2]*Departamento de Química Física, Facultad de Ciencia y Tecnología, Universidad del País Vasco (EHU), Campus de Leioa, Ap. 644, E-48080 Bilbao, Spain*
[3]*Instituto Biofisika (CSIC, EHU), E-48080 Bilbao, Spain*
[4]*Department of Chemistry 'Giacomo Ciamician', University of Bologna, via P. Gobetti, 85, I-40129 Bologna, Italy*
[5]*Interdepartmental Centre for Industrial Aerospace Research (CIRI Aerospace), University of Bologna, via B. Canaccini 12, Forlì, I-47522, Italy*

Accepted 2025 December 4. Received 2025 December 3; in original form 2025 August 1

ABSTRACT

Understanding the presence and distribution of pre-biotic precursors in the interstellar medium (ISM) is key to tracing the chemical origins of life. Among them, 4-oxobutanenitrile ($HCOCH_2CH_2CN$) has been identified in laboratory simulations as a plausible intermediate in the formation of glutamic acid, a proteinogenic amino acid. Here, we report its gas-phase rotational spectrum, measured using two complementary techniques: chirped-pulse Fourier transform microwave (CP-FTMW) spectroscopy (2–18 GHz) and free-jet millimetre-wave (FJ−AMMW) absorption spectroscopy (59.6–80 GHz). Quantum chemical calculations revealed nine low-energy conformers, of which the TC conformer was assigned based on the measured spectra. The resulting spectroscopic parameters were used to search for the molecule in the ultradeep spectral survey of the G+0.693-0.027 molecular cloud, located in the Galactic Center. No signal attributable to 4−oxobutanenitrile was detected. A stringent upper limit to its column density was derived ($N < 4 \times 10^{12}$ cm^{-2}), corresponding to a molecular abundance of $<2.9 \times 10^{-11}$ relative to H_2. This upper limit lies well below the observed abundances of simpler structurally related species containing −HCO and −CN groups, underscoring the challenge of detecting increasingly complex pre-biotic molecules in the ISM and the need for future, more sensitive astronomical facilities.

Key words: astrobiology – astrochemistry – molecular data – methods: laboratory: molecular – ISM: abundances – ISM: molecules.

1 INTRODUCTION

In recent years, our understanding of the chemical complexity in the interstellar medium (ISM) has advanced dramatically. The enhanced sensitivity of modern radiotelescopes – including single-dish facilities such as Yebes 40m, IRAM 30m, and GBT 100m, as well as interferometers like the Atacama Large Millimeter/submillimeter Array (ALMA) – has enabled the detection of an unprecedented number of molecules. Between 2021 and 2025 alone, >105 new species were reported in the ISM, accounting for almost one-third of all known interstellar molecules since the first detection in the late 1930s (P. Swings & L. Rosenfeld 1937). These discoveries have been especially prolific in two chemically rich regions: the dark molecular cloud TMC-1 and the Galactic Center molecular cloud G+0.693-0.027 (hereafter G+0.693). In TMC-1, the newly identified molecules include hydrocarbons (some of them aromatic) such as ortho-benzyne (o-C_6H_4; J. Cernicharo et al. 2021b), or indene (c-C_9H_8; A. M. Burkhardt et al. 2021; J. Cernicharo et al. 2021a); and also CN derivatives such as benzonitrile (c-C_6H_5CN; B. A. McGuire 2018), cyanoacenaphthylene (c-$C_{12}H_7CN$; J. Cernicharo et al. 2024), cyanopyrene (c-$C_{16}H_9CN$; G. Wenzel et al. 2024a, b), and cyanocoronene (c-$C_{24}H_{11}CN$; G. Wenzel et al. 2025). Meanwhile, the G+0.693 cloud has yielded an abundance of complex organic molecules (COMs) containing oxygen (O), nitrogen (N), and sulphur (S). These include alcohols (n-$CH_3CH_2CH_2OH$; I. Jiménez-Serra et al. 2022), diols ($Z-1,2-(CHOH)_2$; V. M. Rivilla et al. 2022c), carboxylic acids (HOCOOH; M. Sanz-Novo et al. 2023), amides (NH_2COCH_2OH; V. M. Rivilla et al. 2023), amines (NH_2OH; V. M. Rivilla et al. 2020b; $NH_2CH_2CH_2OH$; V. M. Rivilla et al. 2021b; CH_2CHNH_2; S. Zeng et al. 2021), imines (Z-HCCCHNH; L. Bizzocchi et al. 2020), isocyanates (C_2H_5NCHO; L. F. Rodríguez-Almeida et al. 2021a), thiols (t-HCOSH and C_2H_5SH; L. F. Rodríguez-Almeida et al. 2021b), and sulphides (CH_3SCH_3; M. Sanz-Novo et al. 2025).

Many of the species discovered towards G+0.693 are considered potential precursors in pre-biotic chemistry. Within the framework

★ E-mail: vrivilla@cab.inta-csic.es (VMR); emiliojose.cocinero@ehu.eus (EJC); sonia.melandri@unibo.it (SM)
† These authors contributed equally to this work.
‡ Current address: Grupo de Espectroscopía Molecular (GEM), Edificio Quifima, Laboratorios de Espectroscopia y Bioespectroscopia, Universidad de Valladolid, E-47011 Valladolid, Spain.

© The Author(s) 2025.
Published by Oxford University Press on behalf of Royal Astronomical Society. This is an Open Access article distributed under the terms of the Creative Commons Attribution License (https://creativecommons.org/licenses/by/4.0/), which permits unrestricted reuse, distribution, and reproduction in any medium, provided the original work is properly cited.

Downloaded from https://academic.oup.com/mnras/article/546/1/staf2224/8384188 by guest on 06 March 2026

of the RNA-world hypothesis (W. Gilbert 1986), which suggests that ribonucleotides were among the first biopolymers to emerge, such compounds play essential roles. Laboratory studies have shown that ribonucleotide building blocks can form under plausible pre-biotic conditions (M. W. Powner, B. Gerland & J. D. Sutherland 2009; B. H. Patel et al. 2015; S. Becker et al. 2019). Their detection in space reinforces the idea that at least part of Earth's early chemical inventory may have originated exogenously. This hypothesis is further supported by the detection of amino acids, nucleobases, and sugars in meteorites (G. Cooper et al. 2001; J. E. Elsila et al. 2016; Y. Furukawa et al. 2019), asteroids (C. Potiszil et al. 2023), and comets (K. Altwegg et al. 2016). This pre-biotic material could have been transferred to our young planet via cometary and meteoritic impacts (J. Oró 1961; J. R. Cronin, S. Pizzarello & D. P. Cruikshank 1988; C. F. Chyba 1990; C. Chyba & C. Sagan 1992; G. Cooper et al. 2001; M. A. Pasek 2008; D. P. Glavin & J. P. Dworkin 2009; B. K. Pearce et al. 2017; B. Marty et al. 2017; D. P. O'Brien et al. 2018; M. Rubin et al. 2019; V. M. Rivilla et al. 2020a). Despite this progress, the exact mechanisms through which complex organics were inherited from the parent molecular cloud remain uncertain. To bridge this gap, it is crucial to identify increasingly complex molecular intermediates in the ISM. However, this quest remains challenging, mainly due to the lack of laboratory spectroscopic data. A strong collaboration between laboratory spectroscopy and observational astronomy is therefore essential. Notably, several detections in G+0.693 arrived closely after their laboratory spectra became available: Z-propynimine (Z-HCCCHNH; L. Bizzocchi et al. 2020), Z-1,2-ethenediol (Z-1,2-$(CHOH)_2$), isobutene ($(CH_3)_2C=CH_2$; M. Fatima et al. 2023), and very recently the tentative identification of 3-hydroxypropanal ($HOCH_2CH_2CHO$; Z. T. P. Fried et al. 2025).

In this work, we present the rotational spectroscopic study 4-oxobutanenitrile ($HCOCH_2CH_2CN$; also know as 3-cyanopropionaldehyde), a molecule proposed in pre-biotic chemistry [see fig. 4(d) in N. Kitadai & S. Maruyama 2018; and also N. M. Grefenstette 2017] as a precursor of glutamic acid, a proteinogenic amino acid fundamental to modern biochemistry. The previous identification towards G+0.693 of other nitriles with 4 carbon atoms (the isomeric family C_4H_3N; V. M. Rivilla et al. 2022b), and the discovery of NO-bearing COMs (e.g. $NH_2CH_2CH_2OH$, $CH_2OH(O)NH_2$; V. M. Rivilla et al. 2021a, 2023, respectively), makes this source an excellent candidate to search for $HCOCH_2CH_2CN$.

After a conformational exploration of the molecule, we characterized its most stable form in the gas phase using broad-band laboratory techniques. The derived spectroscopic parameters enabled a targeted astronomical search towards the G+0.693 molecular cloud, a source renowned for its chemical richness (S. Zeng et al. 2018; V. M. Rivilla et al. 2022b; I. Jimenez-Serra 2025). This study exemplifies the synergy between laboratory spectroscopy and radioastronomical observations in advancing our understanding of chemical complexity in space and guiding future detections of molecular precursors relevant to the RNA-world scenario.

2 METHODS

2.1 Exploration of the conformational space: dihedral scans and energetics

The conformational landscape of 4-oxobutanenitrile was explored by quantum-chemical methods to support the spectroscopic analysis (I. Uriarte et al. 2018; C. Calabrese et al. 2020). The molecule exhibits flexibility around two key dihedral angles, C1-C2-C3-C4 (θ) and C2-C3-C4=O (ϕ), which determine the orientation of its alkyl chain and carbonyl group, respectively. A relaxed two-dimensional potential energy surface (PES) scan was carried out at the B3LYP-D3BJ/def2-TZVPP level using GAUSSIAN 16 (M. E. Frisch et al. 2016) and ORCA (F. Neese et al. 2020). This search identified nine energy minima, arising from combinations of gauche, trans, anticlinal, and cis orientations of the two dihedrals (Fig. 1). All conformers were confirmed by harmonic frequency analysis and corrected for zero-point vibrational energy (ZPE). For the global minimum, TC, the anharmonic approach was also applied by means of the second-order vibrational perturbation theory (VPT2) as implemented in GAUSSIAN 16 (V. Barone 2005; J. Bloino & V. Barone 2012).

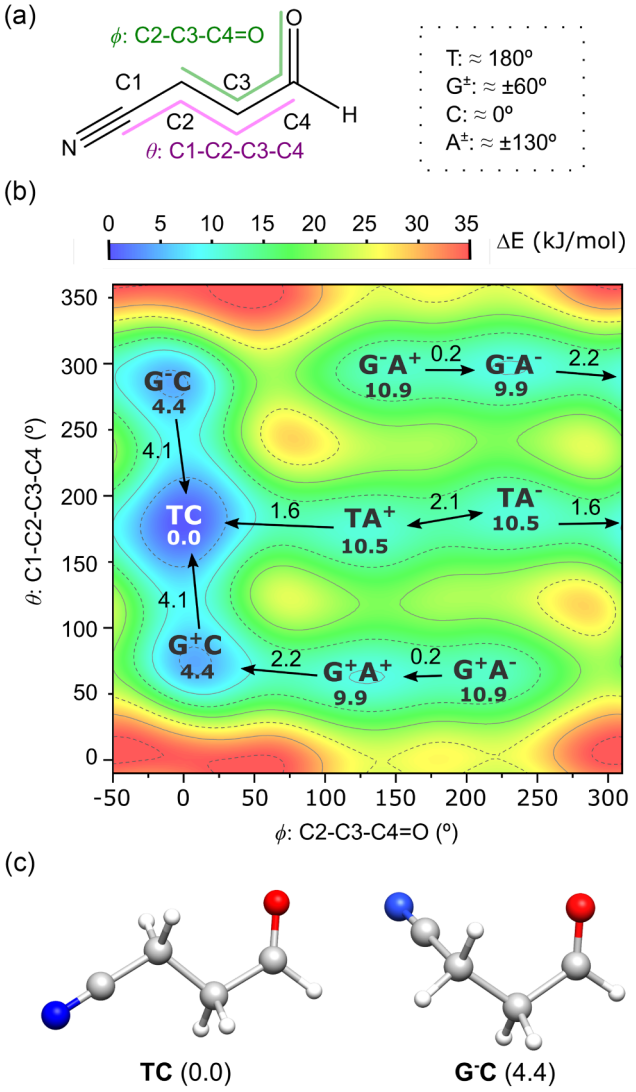


Figure 1. (a) Definition of the torsional angles θ = C1-C2-C3-C4 and ϕ= C2-C3-C4=O used to explore the conformational space of 4-oxobutanenitrile. (b) Relaxed 2D potential energy surface (PES) computed at the B3LYP-D3BJ/def2-TZVPP level showing nine minima. Arrows indicate barriers between key conformers (in kJ mol^{-1}). (c) Optimized geometries of the global minimum TC and the second-lowest conformer G^-C/ G^+C, with their relative energies including ZPE.

The global minimum corresponds to an extended alkyl backbone ($\theta \approx 180°$) and a planar carbonyl group ($\phi \approx 0°$). The remaining eight conformers form four pairs of enantiomers. The first pair, G^-C and G^+C ($\theta \approx \pm 60°$, $\phi \approx 0°$), lies 4.4 kJ mol^{-1} above TC. The other pairs, G^-A^+/G^+A^-, G^-A^-/G^+A^+, and TA^+/TA^-, span relative

Downloaded from https://academic.oup.com/mnras/article/546/1/staf2224/8384188 by guest on 06 March 2026

energies between approximately 10 and 11 kJ mol^{-1} above the global minimum. Transition states connecting these conformers were located using the Nudged Elastic Band – TS method (G. Henkelman, B. P. Uberuaga & H. Jónsson 2000). The barrier between G and C (or the equivalent conformer G^{+}C) to TC is approximately 4.1 kJ mol^{-1}, while all other interconversion barriers were found to be below 3 kJ mol^{-1}. This shallow landscape enables efficient conformational relaxation under supersonic expansion.

2.2 Rotational spectroscopy using CP-FTMW and FJ–AMMW techniques

The rotational spectrum of 4-oxobutanenitrile was recorded using two complementary techniques: chirped-pulse Fourier transform microwave (CP-FTMW) spectroscopy at the University of the Basque Country (I. Uriarte et al. 2016, 2017), and free-jet absorption millimetre-wave (FJ–AMMW) spectroscopy at the University of Bologna (C. Calabrese et al. 2013, 2015 and A. Vigorito et al. 2018).

In the CP-FTMW experiments, the commercial sample was heated to 45° C and seeded in neon at backing pressures of 5−7 bar. The gas mixture was expanded into a high-vacuum chamber (∼ 10^{-6} mbar) through a pulsed nozzle, generating a supersonic molecular beam. Broad-band spectra were recorded in three overlapping frequency windows (2−6.5, 7−14, and 12−18 GHz), each acquired by averaging up to 100 000 free induction decays. The resulting spectra were Fourier transformed to yield high-resolution frequency-domain data.

Measurements in the millimetre-wave region were performed using the FJ–AMMW spectrometer. The sample, maintained at ambient temperature (∼300 K), was entrained in a stream of argon at a stagnation pressure of 19 kPa and expanded through a 0.3 mm pinhole nozzle. The estimated background pressure was ∼0.5 Pa, leading to rotational cooling to 5–10 K. Under these conditions, Doppler-limited absorption signals were recorded in the 59.6−80.0 GHz range with a typical resolution of 50 kHz. Transitions separated by more than 300 kHz were fully resolved. A detailed analysis of selected spectral regions and the assigned transitions is presented in Section 2.3.

Only transitions from the global minimim conformer (TC) were observed, and notably no transitions attributable to the next most stable conformers, G^{+}C or G^{-}C, were detected in either spectrometer. Given the relatively low computed interconversion barrier (∼4.1 kJ mol^{-1} from G^{+}C/G^{-}C to TC), efficient relaxation towards the global minimum is expected during supersonic expansion. This is consistent with experimental trends reported for other flexible molecules, where barriers below ∼4.8 kJ mol^{-1} often lead to full conformational relaxation in the jet (R. Ruoff et al. 1990). To investigate the possible stabilization of metastable species, a second CP-FTMW experiment was carried out using helium (5 bar) instead of neon as carrier gas, averaging over 1.5 million free induction decays in the 8−16 GHz range. However, the resulting spectrum was virtually identical to that obtained with neon, and again only transitions from the TC conformer were observed. These findings confirm that under the jet-cooled conditions employed, 4-oxobutanenitrile undergoes complete relaxation to its global minimum. The combined use of CP-FTMW and FJ–AMMW spectroscopy, providing broad spectral coverage and high-resolution hyperfine structure, enabled the full and unambiguous characterization of the TC conformer.

2.3 Spectral assignment and conformer identification

The rotational spectra of 4-oxobutanenitrile revealed the presence of a single conformer, whose assignment was based on the observation of characteristic μ_a−type R-branch transitions such as $3_{0,3} \leftarrow 2_{0,2}$, $4_{0,4} \leftarrow 3_{0,3}$, and $5_{0,5} \leftarrow 4_{0,4}$. All transitions exhibited hyperfine structure arising from the ^{14}N nuclear quadrupole coupling ($I = 1$). A total of 87 hyperfine components were assigned in the 2−18 GHz region, including μ_b−type transitions and lines up to $J_{up} = 5$ and $K_a = 2$ (see Table 1). In the 59.974−77.666 GHz domain, 16 additional rotational transitions (21 considering hyperfine structure) were identified using FJ–AMMW spectroscopy (Table 1). These included higher-J μ_a− and μ_b−type transitions, extending up to $J_{up} = 20$ and $K_a = 2$. Portion of the spectra in significant regions are shown in Fig. 2. In total, 40 rotational transitions were measured (108 considering hyperfine structure), including 22 μ_a-type R-branch transitions up to J_{up} and $K_a = 2$, 2 μ_b-type P-branch up to $J_{up} = 3$ and 4 μ_b-type Q-branch transitions up to $J = 4$, and 12 μ_b-type R-branch transitions up to $J_{up} = 12$ and $K_a = 2$. The determined spectroscopic constants allow the accurate prediction of μ_a-type R-branch transitions with $K_a = 0$, 1, 2 up to 50 GHz and E_{up} up to 23.1 K. The frequency uncertainties, in velocity units, are in the range 0.05−0.1 km s^{-1}. This enables the search towards the Galactic Center G+0.693-0.027 molecular cloud (see Section 3), which exhibits much larger linewidths (∼15–20 km s^{-1}; M. A. Requena-Torres et al. 2008; V. M. Rivilla et al. 2022b), and where the rotational population is concentrated in the lowest energy levels due to low T_{ex}. The transitions measured here can also assist the identification of Galactic cold clouds with typical linewidths of ∼0.5 km s^{-1} and T_{ex} ∼10 K (e.g. M. Agúndez et al. 2023).

Table 1. Spectroscopic data sets and their contributions to the final fit.

Experiment	Lines[a]	σ[b] (kHz)	J_{up} range	K_a range	Frequency range (GHz)
CP-FTMW	87	12	1−5	0−2	3.122−17.502
FJ–AMMW	21	34	6−20	0−2	59.974−77.666

[a] Considering hyperfine structure; [b] σ is the root mean square deviation of the fit.

For increasing values of J and K, and higher frequencies (up to $J = 99$ and 300 GHz), the frequency predictions naturally show larger uncertainties. For several transitions, including those reaching upper state energies of E_{up} ∼1130 K, the uncertainties still remain <1 km s^{-1}. This accuracy is sufficient to enable searches also towards hot cores, where typical linewidths are 3−8 km^{-1} (e.g. R. Cesaroni et al. 1998; V. M. Rivilla et al. 2017; L. Colzi et al. 2021; A. Belloche et al. 2025). However, for transitions whose predicted uncertainties exceed 1 km s^{-1}, improved frequency values would undoubtedly benefit from additional measurements in the (sub)millimetre wavelength range.

We provide the full line list, including frequency uncertainties, as supplementary material so that the applicability of the predicted frequencies to different kinds of astronomical sources can be easily evaluated. Nevertheless, these uncertainties must be regarded as lower limit estimates, because they only account for the errors of the fitted spectroscopic parameters. They do not include additional contributions such as higher order centrifugal distortion terms, which would be required to obtain more reliable predictions at higher frequencies.

The observed spectrum corresponds unambiguously to the TC conformer, the global minimum identified in our quantum chemical calculations. The theoretical and experimentally derived rotational, quartic centrifugal distortion, and nuclear quadrupole constants are presented in Table 2. All observed lines (Table A1) were fitted using Watson's S-reduced Hamiltonian in the I^r representation (J.

Downloaded from https://academic.oup.com/mnras/article/546/1/staf2224/8384188 by guest on 06 March 2026

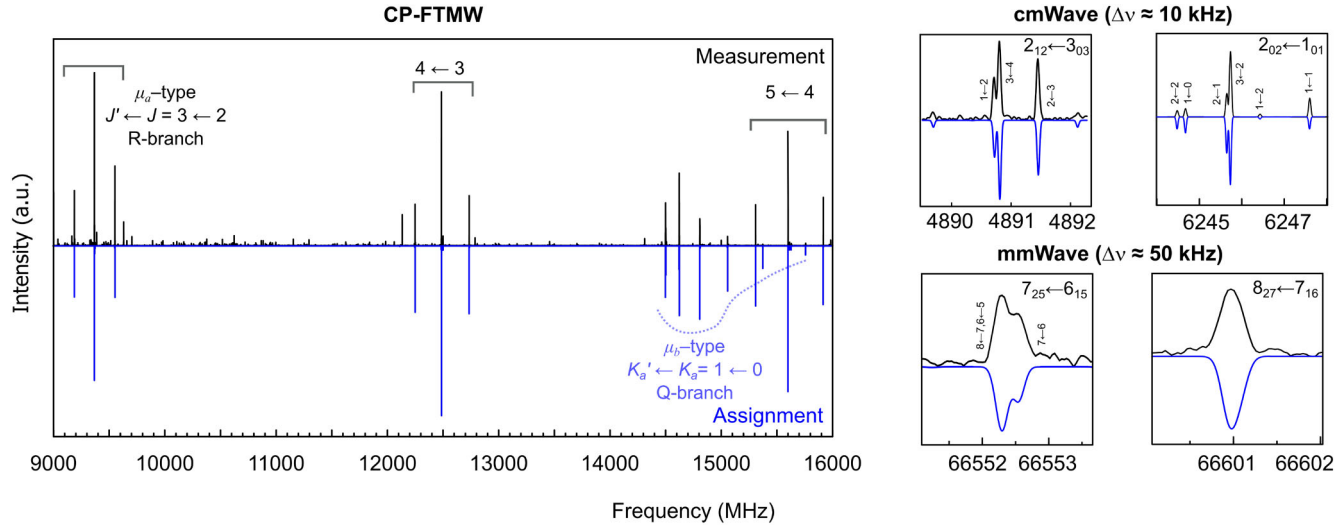


Figure 2. Representative rotational spectrum of 4-oxobutanenitrile assigned to the TC conformer. The main panel shows the broad-band CP-FTMW spectrum in the 9–16 GHz range (black, upper spectrum), featuring μ_a-type R-branch transitions and hyperfine-resolved μ_b-type Q-branch features, together with the fitted spectrum (blue, lower spectrum). The insets on the right display typical transitions measured with each spectrometer: two in the cm-wave range (top) recorded using the CP-FTMW set-up, where the ^{14}N quadrupole hyperfine structure is clearly resolved, and two in the mm-wave region (bottom) from the FJ–AMMW instrument.

Table 2. Calculated and experimental spectroscopic parameters of the observed conformer TC of 4-oxobutanenitrile, derived from a global fit of its rotational transitions recorded in the 2−18 GHz and 59.6−80 GHz ranges.

Parameter	Theory	Experiment
A_0 (MHz)	16103.08	16000.7925(30)
B_0 (MHz)	1608.79	1622.40376(40)
C_0 (MHz)	1490.00	1500.80587(40)
$\frac{3}{2}\chi_{aa}$ (MHz)	−6.60	–5.8503(91)
$\frac{1}{4}(\chi_{bb} - \chi_{cc})$ (MHz)	−0.06	–0.0471(35)
D_J (kHz)	0.193	0.19471(64)
D_{JK} (kHz)	−1.144	–0.925(76)
D_K (kHz)	36.955	36.8(15)
d_1 (kHz)	−0.021	–0.02012(64)
d_2 (kHz)	−0.001	–0.00254(75)
$\lvert\mu_a\rvert$ (D)	2.60	Y
$\lvert\mu_b\rvert$ (D)	1.54	Y
$\lvert\mu_c\rvert$ (D)	0	N

Note. A_0, B_0, and C_0 are the rotational constants in the vibrational ground state (the corresponding equilibrium rotational constants are: $A_e = 16250.00$, $B_e = 1617.95$, $C_e = 1498.13$ MHz); D_J, D_{JK}, D_K, d_1, and d_2 are the quartic centrifugal distortion constants; χ_{aa}, χ_{bb}, and χ_{cc} are the diagonal elements of the ^{14}N nuclear quadrupole coupling tensor; $|\mu_a|$, $|\mu_b|$, and $|\mu_c|$ are the absolute values of the electric dipole moment components along the principal inertial axes (μ_c is zero by symmetry), Y or N denotes that such type of transitions have or have not been observed.

Table 3. Rotational and vibrational partition functions for 4-oxobutanenitrile at different temperatures.

T (K)	Q_{rot}	Q_{vib}
300.000	421710.52	27.6
225.000	273819.18	10.7
150.000	148996.77	4.0
75.000	52665.66	1.6
37.500	18622.36	1.1
18.750	6587.55	1.0
9.375	2331.92	1.0
7.400	1636.43	1.0
3.000	424.42	1.0

K. G. Watson 1977). Its assignment is further supported by the detection of ^{13}C, ^{15}N, and ^{18}O isotopologues in natural abundance ($\sim$ 1.1 per cent, $\sim$ 0.4 per cent, and $\sim$ 0.2 per cent, respectively), with measured transitions (Tables A2–A7) matching those predicted for TC. The rotational constants and nuclear quadrupole coupling constants for the isotopologues are given in the appendix (Table A8). Moreover, in agreement with the C_s symmetry of the TC conformer, no μ_c-type transition lines were observed.

The rotational partition function (Q_{rot}) at different temperatures, reported in Table 3, was evaluated by summing the Boltzmann factors over the energy levels in the ground vibrational state. We used the SPCAT programme (H. M. Pickett 1991) to perform this numerical summation, employing the spectroscopic constants from Table 2 setting maximum frequency 1 THz and J value 200. The vibrational partition function (Q_{vib}), also shown in Table 3, was calculated using the vibrational mode frequencies obtained through the anharmonic approximation (VPT2), employing the B3LYP-D3BJ method and the def2-TZVP basis set, as described in Section 2.1.

The spectroscopic data for all isotopologues, including fitting and prediction files, is offered as supplementary material, and additionally it have been posted into the Strasbourg astronomical Data Center (CDS).

3 INTERSTELLAR SEARCH TOWARDS THE G+0.693−0.027 MOLECULAR CLOUD

To evaluate the presence of 4-oxobutanenitrile in the ISM, we conducted a targeted search towards the G+0.693 molecular cloud, located in the Sgr B2 region of the Galactic Center. This source is well known for its chemical richness and has been a prolific hunting ground for new molecular detections in recent years (V. M. Rivilla et al. 2019, 2020b, 2021b, c, 2022c, a, 2023; L. F. Rodríguez-Almeida et al. 2021b, a; S. Zeng et al. 2021; I. Jiménez-Serra et al. 2022; M. Sanz-Novo et al. 2023, 2024). Our analysis was based on high-sensitivity, broad-band spectral surveys obtained with the National Radio Astronomy Observatory (NRAO) 100m Green Bank telescope (GBT) in West Virginia (USA), and the Yebes

Downloaded from https://academic.oup.com/mnras/article/546/1/staf2224/8384188 by guest on 06 March 2026

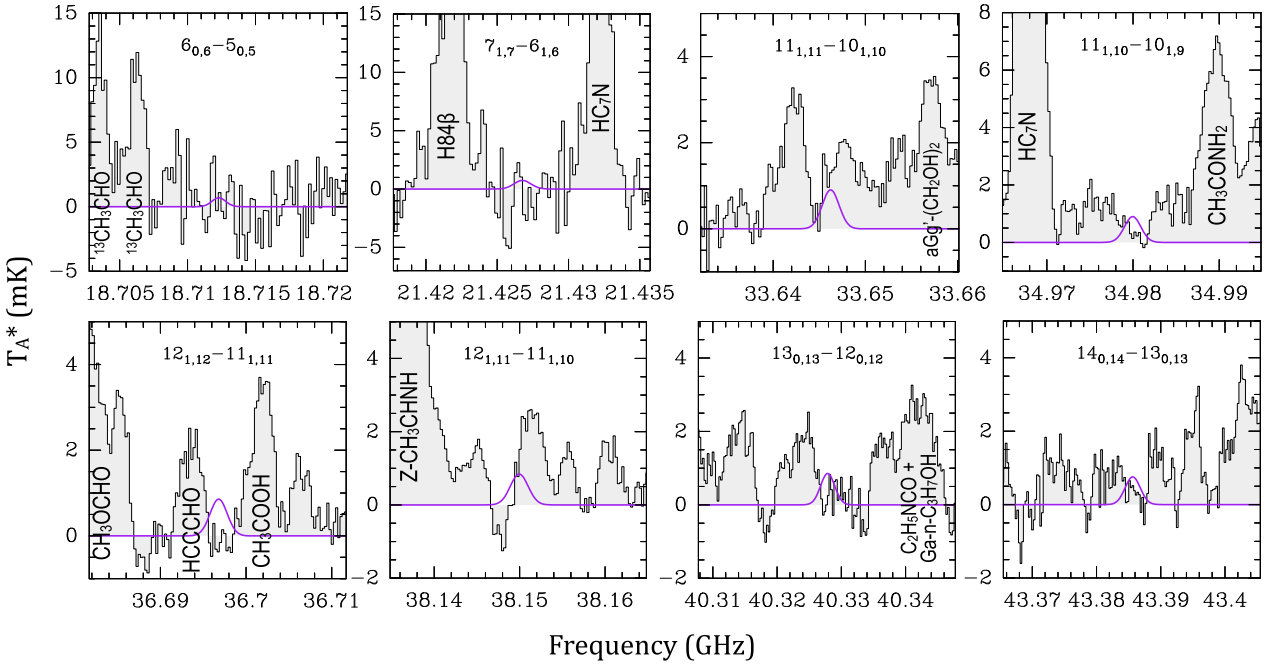


Figure 3. Transitions of $HCOCH_2CH_2CN$ used to compute the column density upper limit towards G+0.693 (see the text). Each panel shows the contribution of three transitions that are not spectrally resolved (see Table 4). The histogram shows the observed spectrum, the purple curve corresponds to the LTE synthetic model of $HCOCH_2CH_2CN$ using the column density upper limit derived in this work. Transitions of other species identified in the survey are labelled.

40m telescope (Guadalajara, Spain). These observations cover the spectral regions where the strongest transitions of $HCOCH_2CH_2CN$ at the typical excitation temperatures of G+0.693 ($\sim 5-20$ K) are predicted. Further observational details, including frequency coverage, spectral resolution, and beam sizes, are given in S. Zeng et al. (2018) and V. M. Rivilla et al. (2023). Given the extended nature of the molecular emission in G+0.693 (e.g. S. Brünken et al. 2010; P. A. Jones et al. 2012; J. Li et al. 2020; M. G. Santa-Maria et al. 2021; L. Colzi et al. 2024), all intensities were expressed in the T_A^* scale.

We implemented the newly derived spectroscopic parameters of $HCOCH_2CH_2CN$ into the MADCUBA package[1] (S. Martín et al. 2019). We generated the Local Thermodynamic Equilibrium (LTE) synthetic spectra using the SLIM (Spectral Line Identification and Modeling) tool of MADCUBA, which were compared to the observational data. We note that, given the low excitation temperatures of the molecules in G+0.693, we did not include the vibrational contribution to the partition function (Q_{vib}) in this case. No signals attributable to $HCOCH_2CH_2CN$ were found. To derive an upper limit to the column density, we selected the most intense and least blended transitions predicted by the LTE model. These transitions (all μ_a-type R-branch) fall within the frequency ranges highlighted in Fig. 3, with root mean square (rms) noise levels of $\sim$2.3 mK for the GBT data, and 0.4−1 mK for the Yebes data. The selected transitions appear as groups of three unresolved hyperfine components (see Table 4). The LTE simulations assumed excitation parameters consistent with previous fits to other nitrile- and formyl-bearing species in the same source, specifically $T_{ex} = 7.4$ K, $v_{LSR} = 68$ km s,$^{-1}$ and full width at half-maximum (FWHM) = 19.2 km s^{-1} (V. M. Rivilla et al. 2022b). Using this model, we computed the maximum column

[1]Madrid Data Cube Analysis on ImageJ is a software developed at the Center of Astrobiology (CAB) in Madrid; http://cab.inta-csic.es/madcuba/.

Table 4. Selected transitions of $HCOCH_2CH_2CN$ used to compute the column density upper limit in the G+0.693−0.027 molecular cloud (see Fig. 3). Each group of three entries corresponds to unresolved hyperfine components of a rotational transition. Frequencies, intensities (at 300 K), and upper-state energies were calculated using the spectroscopic parameters derived in this work. Numbers in parenthesis in the frequency values give the uncertainty on the last digits.

Frequency (GHz)	Transition J_{K_a,K_c} F	log I (nm^2 MHz)	g_u	E_{up} (K)
18.7122133(34)	$6_{0,6}$ 5–$5_{0,5}$ 4	−6.740	11	3.1
18.7122421(34)	$6_{0,6}$ 6–$5_{0,5}$ 5	−6.666	13	3.1
18.7122578(34)	$6_{0,6}$ 7–$5_{0,5}$ 6	−6.591	15	3.1
21.4267372(48)	$7_{1,7}$ 7–$6_{1,6}$ 6	−6.489	15	4.8
21.4267461(48)	$7_{1,7}$ 6–$6_{1,6}$ 5	−6.552	13	4.8
21.4267730(48)	$7_{1,7}$ 8–$6_{1,6}$ 7	−6.426	17	4.8
33.6463327(89)	$11_{1,11}$ 10–$10_{1,10}$ 9	−5.937	21	10.4
33.6463327(89)	$11_{1,11}$ 11–$10_{1,10}$ 10	−5.898	23	10.4
33.6463445(89)	$11_{1,11}$ 12–$10_{1,10}$ 11	−5.858	25	10.4
34.9798050(83)	$11_{1,10}$ 10–$10_{1,9}$ 9	−5.864	21	10.8
34.9798054(83)	$11_{1,10}$ 11–$10_{1,9}$ 10	−5.904	23	10.8
34.9798166(83)	$11_{1,10}$ 12–$10_{1,9}$ 11	−5.824	25	10.8
36.6969490(104)	$12_{1,12}$ 11–$11_{1,11}$ 10	−5.822	23	12.1
36.6969494(104)	$12_{1,12}$ 12–$11_{1,11}$ 11	−5.786	25	12.1
36.6969590(104)	$12_{1,12}$ 13–$11_{1,11}$ 12	−5.749	27	12.1
38.1498001(96)	$12_{1,11}$ 11–$11_{1,10}$ 10	−5.789	23	12.6
38.1498001(96)	$12_{1,11}$ 12–$11_{1,10}$ 11	−5.753	25	12.6
38.1498095(96)	$12_{1,11}$ 13–$11_{1,10}$ 12	−5.716	27	12.6
40.3279643(100)	$13_{0,13}$ 12–$12_{0,12}$ 11	−5.701	25	13.6
40.3279678(100)	$13_{0,13}$ 13–$12_{0,12}$ 12	−5.668	27	13.6
40.3279731(100)	$13_{0,13}$ 14–$12_{0,12}$ 13	−5.634	29	13.6
43.3857819(118)	$14_{0,14}$ 13–$13_{0,13}$ 12	−5.605	27	15.7
43.3857846(118)	$14_{0,14}$ 14–$13_{0,13}$ 13	−5.575	29	15.7
43.3857895(118)	$14_{0,14}$ 15–$13_{0,13}$ 14	−5.543	31	15.7

Downloaded from https://academic.oup.com/mnras/article/546/1/staf2224/8384188 by guest on 06 March 2026

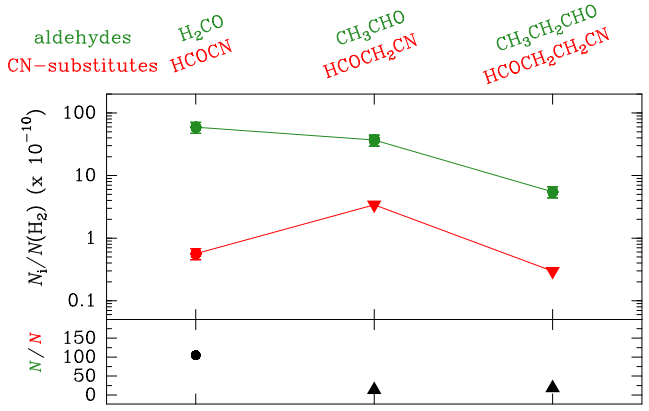


Figure 4. Upper panel: molecular abundances of aldehydes detected towards G+0.693 − formaldehyde, acetaldehyde, and propionaldehyde (propanal) − from I. Jiménez-Serra et al. (2020), V. M. Rivilla et al. (2020b), M. Sanz-Novo et al. (2022); compared to those of their CN−substitutes − oxoacetonitrile, 3-oxopropanenitrile and 4-oxobutanenitrile − from V. M. Rivilla et al. (2022b) and this work. An uncertainty of 20 per cent for the molecular abundances has been assumed. Upper limits are denoted with downward-pointing triangles. Lower panel: column density molecular ratio of the aldehyde/CN−substitute pairs. Lower limits are denoted with upward-pointing triangles.

density (N) consistent with the absence of detectable signal, yielding a conservative upper limit of $N < 4 \times 10^{12}$ cm^{-2}. This corresponds to a molecular abundance of $<2.9 \times 10^{-11}$ relative to H_2, adopting $N(H_2) = 1.35 \times 10^{23}$ cm^{-2} (S. Martín et al. 2008). We note that this abundance upper limit is significantly lower, by a factor of 9, than that derived previously for the simpler 3-oxopropanenitrile ($HCOCH_2CN$; V. M. Rivilla et al. 2022b).

4 DISCUSSION: ASTRONOMICAL IMPLICATIONS

The derived upper limit for the molecular abundance of $HCOCH_2CH_2CN$ (11 atoms) indicates that it is significantly less abundant than the largest species detected so far towards G+0.693, which are ethanolamine ($NH_2CH_2CH_2OH$, 11 atoms; V. M. Rivilla et al. 2021b), and n−propanol ($CH_3CH_2CH_2OH$, 12 atoms; I. Jiménez-Serra et al. 2022), whose abundances are of several 10^{-10}. To place the derived upper limit in context, we compared with other structurally similar species. $HCOCH_2CH_2CN$ can be seen as the CN−substitute of the interstellar molecule propionaldehyde (CH_3CH_2CHO, also known as propanal). Similarly, the CN−substitutes of two abundant interstellar aldehydes, formaldehyde (H_2CO), and acetaldehyde (CH_3CHO), are oxoacetonitrile (HCOCN) and 3-oxopropanenitrile ($HCOCH_2CN$). To test observationally how efficient is the −CN substitution of aldehydes in the ISM, we compare in Fig. 4 the abundances derived towards G+0.693 of these aldehydes (from I. Jiménez-Serra et al. 2020; V. M. Rivilla et al. 2020b; M. Sanz-Novo et al. 2022) with the values (or upper limits) of their CN−substitutes (from V. M. Rivilla et al. 2022b and this work). The abundances of aldehydes decrease with increasing complexity, as observed in other families of molecules towards G+0.693 (alcohols, isocyanates, thiols; L. F. Rodríguez-Almeida et al. 2021a, b; I. Jiménez-Serra et al. 2022). Assuming that the H_2CO/HCOCN ratio of ∼100 (Fig. 4) is similar for the more complex aldehyde/CN−substitute pairs, the expected abundances for $HCOCH_2CN$ and $HCOCH_2CH_2CN$ would be at least one order of magnitude lower than the upper limits derived (see Fig. 4). These low abundances are well below the current sensitivity limits of the astronomical observations.

To infer the expected abundance of $HCOCH_2CH_2CN$ in the ISM, and therefore to open the possibility for its future detection, we need to consider the viability of possible chemical routes working at interstellar conditions. There are not, to our knowledge, theoretical and/or experimental works devoted to the interstellar synthesis of $HCOCH_2CH_2CN$. We discuss here some possible chemical pathways, based on previous studies of simpler CN−substitutes of aldehydes. The quantum chemical calculations by F. Tonolo et al. (2020) showed that HCOCN can be efficiently formed through the gas-phase reaction between H_2CO and the CN radical. Therefore, one might think that the reactions of CN with CH_3CHO and CH_3CH_2CHO can form $HCOCH_2CN$ and $HCOCH_2CH_2CN$, respectively. However, F. Tonolo et al. (2020) also showed that CN + CH_3CHO has two possible product paths: (i) HCOCN + CH_3 and (ii) H + acetyl cyanide ($CH_3C(O)CN$), an isomer of $HCOCH_2CN$. Acetyl cyanide is formed through the CN attack on to the unsaturated carbon of CH_3CHO, while the formation of $HCOCH_2CN$ would need the CN attack on to the saturated carbon of the methyl group, which is not favoured according to F. Tonolo et al. (2020) calculations. It was also demonstrated in other systems that the CN attack on to unsaturated carbons are dominant (e.g. N. Balucani et al. 2000). It is therefore unlikely that the gas-phase reaction between CN and CH_3CH_2CHO conducts to the formation of $HCOCH_2CH_2CN$.

A possible alternative is the reaction of CN with propylene oxide, $CH_3(O)CHCH_3$. The analogous reaction with ethylene oxide (c-C_2H_4O) produces $HCOCH_2CN$ + H (S. Alessandrini & M. Melosso 2021), although the main reaction pathway is 2-oxiranyl radical + HCN. Since propylene oxide has been identified in the ISM (B. A. McGuire et al. 2016), we encourage new theoretical calculations to study in detail whether its reaction with CN can form $HCOCH_2CH_2CN$ at a significant rate.

Within a broader view of the chemical content in G+0.693, we also compared the upper limits derived for $HCOCH_2CH_2CN$ with other nitrile- and formyl-containing species detected (or searched for) towards G+0.693 in previous works. These include formic acid (HCOOH, *trans*-conformer; L. F. Rodríguez-Almeida et al. 2021b), cyanoformaldehyde (HCOCN; V. M. Rivilla et al. 2022b), thioformic-acid (HCOSH, *trans*-conformer; L. F. Rodríguez-Almeida et al. 2021b), glycolaldehyde ($HCOCH_2OH$; V. M. Rivilla et al. 2022c), ethylcyanide (CH_3CH_2CN; S. Zeng et al. 2018), glycolonitrile ($HOCH_2CN$; V. M. Rivilla et al. 2022b), and 3-oxopropanenitrile ($HCOCH_2CN$; V. M. Rivilla et al. 2022b). As shown in Fig. 5, the abundance constraint for $HCOCH_2CH_2CN$ is the lowest. This underscores again the importance of even more sensitive observations to detect the next tier of interstellar complexity, especially molecules with plausible links to pre-biotic chemistry. Completing the inventory of –CN and HCO-bearing compounds in chemically rich regions like G+0.693 will help refine models for the emergence of molecular complexity in space.

5 CONCLUSIONS AND OUTLOOK

We have investigated the rotational spectra of 4-oxobutanenitrile ($HCOCH_2CH_2CN$), a proposed precursor of glutamic acid, an amino acid essential for protein biosynthesis. Through quantum chemical calculations, we mapped its conformational space, identifying nine stable minima. The global minimum conformer was confirmed experimentally, and its rotational spectrum was recorded in the 2−18 and 59.6−80 GHz regions with high resolution, enabling its astronomical search towards the G+0.693–0.027 molecular cloud,

Downloaded from https://academic.oup.com/mnras/article/546/1/staf2224/8384188 by guest on 06 March 2026

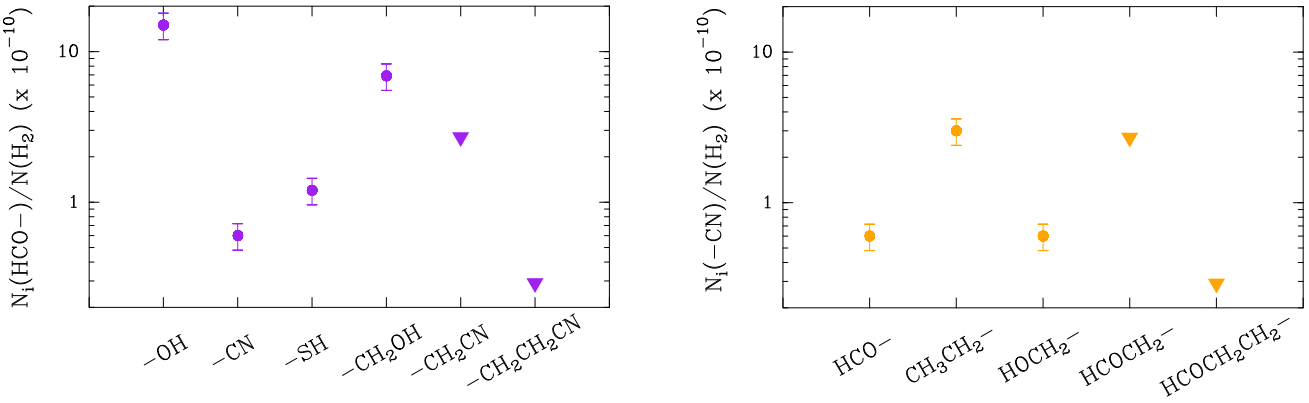


Figure 5. Molecular abundances derived towards the G+0.693 molecular cloud of molecules containing the formyl group (−HCO, left panel), and the nitrile group (−CN, right panel), based on the values reported in this work and S. Zeng et al. (2018), L. F. Rodríguez-Almeida et al. (2021b), and V. M. Rivilla et al. (2022b, 2022c). An uncertainty of 20 per cent for the molecular abundances has been assumed. Upper limits are denoted with downward-pointing triangles.

located in the Sgr B2 complex. The molecule was not detected, and we derived a stringent upper limit to its column density of $N < 4 \times 10^{12}$ cm^{-2}, corresponding to a fractional abundance of $<2.9 \times 10^{-11}$ relative to H_2. This upper limit is significantly lower than the derived abundances of chemically similar species containing −HCO and −CN groups, and also lower than those of the most complex species detected so far towards this cloud. We have discussed the viability of several chemical pathways to form this molecule in the ISM, aiming to pave the way for a future detection. Our findings reinforce the need to enhance the sensitivity of current radioastronomical instrumentation to access a new generation of elusive molecular species. Such efforts are essential to expand our inventory of pre-biotic molecules in the ISM and to deepen our understanding of the chemical steps that may lead towards the emergence of life.

ACKNOWLEDGEMENTS

We are very grateful to the Yebes 40 m and IRAM 30 m telescope staff for their precious help during the different observing runs. The 40 m radio telescope at Yebes Observatory is operated by the Spanish Geographic Institute (IGN; Ministerio de Transportes, Movilidad y Agenda Urbana). VMR and IJ-S acknowledge support from the grant No. PID2022-136814NB-I00 by the Spanish Ministry of Science, Innovation and Universities/State Agency of Research MCIU/AEI/10.13039/501100011033 and by ERDF, UE. VMR also acknowledges support from the grant PID2022-136814NB-I00 by the Spanish Ministry of Science, Innovation and Universities/State Agency of Research MICIU/AEI/10.13039/501100011033 and by ERDF, UE; the grant RYC2020-029387-I funded by MICIU/AEI/10.13039/501100011033 and by 'ESF, Investing in your future', and from the Consejo Superior de Investigaciones Científicas (CSIC) and the Centro de Astrobiología (CAB) through the project 20225AT015 (Proyectos intramurales especiales del CSIC); and from the grant CNS2023-144464 funded by MICIU/AEI/10.13039/501100011033 and by 'European Union NextGenerationEU/PRTR'. WS acknowledges a post-doctoral fellowship under the MUR PRIN national project (grant no. J43C21000050001). EJC and FJB acknowledge financial support from the Spanish Ministry of Science, Innovation and Universities (MICIU/AEI, project PID2023-147698NB-I00) and from the Basque Government (project IT1491-22). AI acknowledges a post-doctoral fellowship from the Basque Government. The authors also acknowledge the use of computational resources provided by SGIker (UPV/EHU) and CESGA. SM and AM acknowledge financial support from the Italian Space Agency, ASI, and the Ministry of University and Research, MUR, through the Space It Up project funded under contract no. 2024-5-E.0 – CUP no. I53D24000060005. The authors also thank the University of Bologna for financial support through the RFO project. IJ-S acknowledges funding from the ERC CoG grant OPENS (project number 101125858) funded by the European Union.

DATA AVAILABILITY

The observational data of the G+0.693–0.027 spectral survey used in this article will be shared on reasonable request to vrivilla@cab.inta-csic.es. The spectroscopic data, including fitting and prediction files, is offered as supplementary material.

REFERENCES

Agúndez M., Marcelino N., Tercero B., Jiménez-Serra I., Cernicharo J., 2023, A&A, 677, A106
Alessandrini S., Melosso M., 2021, Front. Astron. Space Sci., 8, 159
Altwegg K. et al., 2016, Sci. Adv., 2, e1600285
Balucani N., Asvany O., Huang L. C. L., Lee Y. T., Kaiser R. I., Osamura Y., Bettinger H. F., 2000, ApJ, 545, 892
Barone V., 2005, J. Chem. Phys., 122, 014108
Becker S. et al., 2019, Science, 366, 76
Belloche A., Garrod R. T., Müller H. S. P., Morin N. J., Willis S. A., Menten K. M., 2025, A&A, 698, A143
Bizzocchi L. et al., 2020, A&A, 640, A98
Bloino J., Barone V., 2012, J. Chem. Phys., 136, 124108
Brünken S., Belloche A., Martín S., Verheyen L., Menten K. M., 2010, A&A, 516, A109
Burkhardt A. M. et al., 2021, ApJ, 913, L18
Calabrese C., Maris A., Evangelisti L., Favero L. B., Melandri S., Caminati W., 2013, J. Phys. Chem. A, 117, 13712
Calabrese C., Vigorito A., Maris A., Mariotti S., Fathi P., Geppert W. D., Melandri S., 2015, J. Phys. Chem. A, 119, 11674
Calabrese C. et al., 2020, ACS Central Sci., 6, 293
Cernicharo J., Agúndez M., Cabezas C., Tercero B., Marcelino N., Pardo J. R., de Vicente P., 2021a, A&A, 649, L15
Cernicharo J., Agúndez M., Kaiser R. I., Cabezas C., Tercero B., Marcelino N., Pardo J. R., de Vicente P., 2021b, A&A, 652, L9
Cernicharo J. et al., 2024, A&A, 690, L13

Downloaded from https://academic.oup.com/mnras/article/546/1/staf2224/8384188 by guest on 06 March 2026

Cesaroni R., Hofner P., Walmsley C. M., Churchwell E., 1998, A&A, 331, 709
Chyba C. F., 1990, Nature, 343, 129
Chyba C., Sagan C., 1992, Nature, 355, 125
Colzi L. et al., 2021, A&A, 653, A129
Colzi L. et al., 2024, A&A, 690, A121
Cooper G., Kimmich N., Belisle W., Sarinana J., Brabham K., Garrel L., 2001, Nature, 414, 879
Cronin J. R., Pizzarello S., Cruikshank D. P., 1988, in Kerridge J. F., Matthews M. S., eds, Meteorites and the Early Solar System. Univ. Arizona Press, Tucson, p. 819
Elsila J. E., Aponte J. C., Blackmond D. G., Burton A. S., Dworkin J. P., Glavin D. P., 2016, ACS Cent. Sci., 2, 370
Fatima M., Müller H. S. P., Zingsheim O., Lewen F., Rivilla V. M., Jiménez-Serra I., Martín-Pintado J., Schlemmer S., 2023, A&A, 680, A25
Fried Z. T. P. et al., 2025, ApJ, 992, 187
Frisch M. J. et al., 2016, Gaussian 16, Revision C.01, Gaussian, Inc., Wallingford CT
Furukawa Y., Chikaraishi Y., Ohkouchi N., Ogawa N. O., Glavin D. P., Dworkin J. P., Abe C., Nakamura T., 2019, Proc. Natl. Acad. Sci., 116, 24440
Gilbert W., 1986, Nature, 319, 618
Glavin D. P., Dworkin J. P., 2009, Proc. Natl. Acad. Sci., 106, 5487
Grefenstette N. M., 2017, PhD thesis, UCL (University College London)
Henkelman G., Uberuaga B. P., Jónsson H., 2000, J. Chem. Phys., 113, 9901
Jimenez-Serra I., 2025, preprint (arXiv:2501.01782)
Jiménez-Serra I. et al., 2020, Astrobiology, 20, 1048
Jiménez-Serra I. et al., 2022, A&A, 663, A181
Jones P. A. et al., 2012, MNRAS, 419, 2961
Kitadai N., Maruyama S., 2018, Geosci. Front., 9, 1117
Li J. et al., 2020, MNRAS, 492, 556
Martín S., Requena-Torres M. A., Martín-Pintado J., Mauersberger R., 2008, ApJ, 678, 245
Martín S., Martín-Pintado J., Blanco-Sánchez C., Rivilla V. M., Rodríguez-Franco A., Rico-Villas F., 2019, A&A, 631, A159
Marty B. et al., 2017, Science, 356, 1069
McGuire B. A., 2018, ApJS, 239, 17
McGuire B. A., Carroll P. B., Loomis R. A., Finneran I. A., Jewell P. R., Remijan A. J., Blake G. A., 2016, Science, 352, 1449
Neese F., Wennmohs F., Becker U., Riplinger C., 2020, J. Chem. Phys., 152, 224108
O'Brien D. P., Izidoro A., Jacobson S. A., Raymond S. N., Rubie D. C., 2018, Space Sci. Rev., 214, 47
Oró J., 1961, Nature, 190, 389
Pasek M. A., 2008, Proc. Natl. Acad. Sci., 105, 853
Patel B. H., Percivalle C., Ritson D. J., Duffy C. D., Sutherland J. D., 2015, Nat. Chem., 7, 301
Pearce B. K., Pudritz R. E., Semenov D. A., Henning T. K., 2017, Proc. Natl. Acad. Sci., 114, 11327
Pickett H. M., 1991, J. Mol. Spectrosc., 148, 371
Potiszil C. et al., 2023, Nat. Commun., 14, 1482
Powner M. W., Gerland B., Sutherland J. D., 2009, Nature, 459, 239
Requena-Torres M. A., Martín-Pintado J., Martín S., Morris M. R., 2008, ApJ, 672, 352
Rivilla V. M., Beltrán M. T., Cesaroni R., Fontani F., Codella C., Zhang Q., 2017, A&A, 598, A59
Rivilla V. M. et al., 2019, MNRAS, 483, L114
Rivilla V. M. et al., 2020a, MNRAS, 492, 1180
Rivilla V. M. et al., 2020b, ApJ, 899, L28
Rivilla V. M. et al., 2021a, Proc. Natl. Acad. Sci., 118, e2101314118
Rivilla V. M. et al., 2021b, Proc. Natl. Acad. Sci., 118, 2101314118
Rivilla V. M. et al., 2021c, MNRAS, 506, L79
Rivilla V. M. et al., 2022a, Front. Astron. Space Sci., 9, 829288
Rivilla V. M. et al., 2022b, Front. Astron. Space Sci., 9, 876870
Rivilla V. M. et al., 2022c, ApJ, 929, L11
Rivilla V. M. et al., 2023, ApJ, 953, L20
Rodríguez-Almeida L. F. et al., 2021a, A&A, 654, L1
Rodríguez-Almeida L. F. et al., 2021b, ApJ, 912, L11
Rubin M., Bekaert D. V., Broadley M. W., Drozdovskaya M. N., Wampfler S. F., 2019, ACS Earth Space Chem., 3, 1792
Ruoff R., Klots T., Emilsson T., Gutowsky H., 1990, J. Chem. Phys., 93, 3142
Santa-Maria M. G., Goicoechea J. R., Etxaluze M., Cernicharo J., Cuadrado S., 2021, A&A, 649, A32
Sanz-Novo M. et al., 2022, A&A, 666, A114
Sanz-Novo M. et al., 2023, ApJ, 954, 3
Sanz-Novo M. et al., 2024, ApJ, 965, 149
Sanz-Novo M. et al., 2025, ApJ, 980, L37
Swings P., Rosenfeld L., 1937, ApJ, 86, 483
Tonolo F., Lupi J., Puzzarini C., Barone V., 2020, ApJ, 900, 85
Uriarte I. et al., 2016, Phys. Chem. Chem. Phys., 18, 3966
Uriarte I., Pérez C., Caballero-Mancebo E., Basterretxea F. J., Lesarri A., Fernández J. A., Cocinero E. J., 2017, Chem.–A Eur. J., 23, 7238
Uriarte I., Melandri S., Maris A., Calabrese C., Cocinero E. J., 2018, J. Phys. Chem. Lett., 9, 1497
Vigorito A., Calabrese C., Melandri S., Caracciolo A., Mariotti S., Giannetti A., Massardi M., Maris A., 2018, A&A, 619, A140
Watson J. K. G., 1977, in Durig J. R., ed., Vibrational Spectra and Structure, Vol. 6. Elsevier, Amsterdam, p. 1
Wenzel G. et al., 2024a, Nat. Astron., 9, 262
Wenzel G. et al., 2024b, Science, 386, 810
Wenzel G. et al., 2025, ApJ, 984, L36
Zeng S. et al., 2018, MNRAS, 478, 2962
Zeng S. et al., 2021, ApJ, 920, L27

SUPPORTING INFORMATION

Supplementary data are available at *MNRAS* online.

4oxobutanenitrile

Please note: Oxford University Press is not responsible for the content or functionality of any supporting materials supplied by the authors. Any queries (other than missing material) should be directed to the corresponding author for the article.

APPENDIX A: ROTATIONAL SPECTROSCOPY DATA

Downloaded from https://academic.oup.com/mnras/article/546/1/staf2224/8384188 by guest on 06 March 2026

Table A1. Measured rotational transition frequencies and corresponding deviations from the model of the TC conformer of 4-oxobutanenitrile.

$J'_{K'_a,K'_c}$ F'	$J''_{K''_a,K''_c}$ F''	Freq. (MHz)	o.-c. (MHz)	$J'_{K'_a,K'_c}$ F'	$J''_{K''_a,K''_c}$ F''	Freq. (MHz)	o.-c. (MHz)
$1_{0,1}$ 1	$0_{0,0}$ 1	3122.233	−0.001	$1_{1,0}$ 1	$1_{0,1}$ 2	14500.270	0.002
$1_{0,1}$ 2	$0_{0,0}$ 1	3123.406	0.002	$1_{1,0}$ 2	$1_{0,1}$ 1	14500.825	0.001
$1_{0,1}$ 0	$0_{0,0}$ 1	3125.162	0.003	$1_{1,0}$ 1	$1_{0,1}$ 1	14501.442	0.005
$2_{0,2}$ 1	$1_{0,1}$ 0	6244.671	0.000	$2_{1,1}$ 2	$2_{0,2}$ 1	14620.883	0.002
$2_{0,2}$ 2	$1_{0,1}$ 2	6244.475	0.001	$2_{1,1}$ 2	$2_{0,2}$ 3	14621.576	−0.002
$2_{0,2}$ 3	$1_{0,1}$ 2	6245.731	0.003	$2_{1,1}$ 1	$2_{0,2}$ 1	14621.811	0.001
$2_{0,2}$ 2	$1_{0,1}$ 1	6245.646	0.001	$2_{1,1}$ 3	$2_{0,2}$ 3	14622.171	−0.003
$2_{0,2}$ 1	$1_{0,1}$ 2	6246.427	0.002	$2_{1,1}$ 2	$2_{0,2}$ 2	14622.831	−0.001
$2_{0,2}$ 1	$1_{0,1}$ 1	6247.598	0.002	$2_{1,1}$ 3	$2_{0,2}$ 2	14623.429	0.001
$2_{1,2}$ 2	$1_{1,1}$ 1	6123.849	0.004	$2_{1,1}$ 1	$2_{0,2}$ 2	14623.759	−0.002
$2_{1,2}$ 2	$1_{1,1}$ 2	6124.403	0.002	$3_{1,2}$ 3	$3_{0,3}$ 2	14805.824	0.001
$2_{1,2}$ 1	$1_{1,1}$ 1	6124.873	0.006	$3_{1,2}$ 3	$3_{0,3}$ 4	14806.271	−0.007
$2_{1,2}$ 3	$1_{1,1}$ 2	6125.064	0.005	$3_{1,2}$ 2	$3_{0,3}$ 2	14807.084	−0.013
$2_{1,2}$ 1	$1_{1,1}$ 0	6126.264	0.005	$3_{1,2}$ 4	$3_{0,3}$ 4	14807.231	0.009
$2_{1,1}$ 2	$1_{1,0}$ 1	6367.036	−0.003	$3_{1,2}$ 3	$3_{0,3}$ 3	14807.582	0.004
$2_{1,1}$ 3	$1_{1,0}$ 2	6368.254	0.005	$3_{1,2}$ 4	$3_{0,3}$ 3	14808.525	0.003
$2_{1,1}$ 1	$1_{1,0}$ 0	6369.504	0.004	$3_{1,2}$ 2	$3_{0,3}$ 3	14808.855	0.002
$3_{0,3}$ 3	$2_{0,2}$ 3	9365.283	0.002	$4_{1,3}$ 4	$4_{0,4}$ 5	15055.498	0.016
$3_{0,3}$ 2	$2_{0,2}$ 1	9366.345	0.004	$4_{1,3}$ 5	$4_{0,4}$ 5	15056.614	0.034
$3_{0,3}$ 3	$2_{0,2}$ 2	9366.514	−0.021	$4_{1,3}$ 4	$4_{0,4}$ 4	15056.829	0.017
$3_{0,3}$ 4	$2_{0,2}$ 3	9366.609	0.027	$4_{1,3}$ 5	$4_{0,4}$ 4	15057.899	−0.011
$3_{0,3}$ 2	$2_{0,2}$ 2	9368.295	0.004	$4_{1,3}$ 3	$4_{0,4}$ 4	15058.201	0.008
$3_{1,3}$ 3	$2_{1,2}$ 3	9185.837	−0.002	$1_{1,1}$ 0	$0_{0,0}$ 1	17500.635	0.000
$3_{1,3}$ 3	$2_{1,2}$ 2	9186.499	0.003	$1_{1,1}$ 2	$0_{0,0}$ 1	17501.467	−0.003
$3_{1,3}$ 4,2	$2_{1,2}$ 3,1	9186.850	0.011	$1_{1,1}$ 1	$0_{0,0}$ 1	17502.021	−0.005
$3_{1,3}$ 2	$2_{1,2}$ 2	9187.863	0.008	$2_{1,2}$ 1	$3_{0,3}$ 2	4890.715	−0.008
$3_{1,2}$ 3	$2_{1,1}$ 3	9550.696	0.010	$2_{1,2}$ 3	$3_{0,3}$ 4	4890.805	−0.009
$3_{1,2}$ 3	$2_{1,1}$ 2	9551.292	0.010	$2_{1,2}$ 2	$3_{0,3}$ 3	4891.448	−0.009
$3_{1,2}$ 2,4	$2_{1,1}$ 1,3	9551.640	0.011	$1_{1,1}$ 0	$2_{0,2}$ 1	8130.801	−0.005
$3_{1,2}$ 2	$2_{1,1}$ 2	9552.569	0.013	$1_{1,1}$ 1	$2_{0,2}$ 1	8132.190	−0.008
$3_{2,1}$ 4	$2_{2,0}$ 3	9372.956	−0.024	$1_{1,1}$ 2	$2_{0,2}$ 3	8132.331	−0.006
$3_{2,2}$ 4	$2_{2,1}$ 3	9369.891	−0.018	$1_{1,1}$ 2	$2_{0,2}$ 2	8133.586	−0.005
$4_{0,4}$ 4	$3_{0,3}$ 4	12483.821	0.012	$1_{1,1}$ 1	$2_{0,2}$ 2	8134.142	−0.006
$4_{0,4}$ 5	$3_{0,3}$ 4	12485.141	0.001	$6_{2,4}$ 5,7	$5_{1,5}$ 4,6	63021.33	−0.03
$4_{0,4}$ 3	$3_{0,3}$ 3	12486.785	0.003	$6_{2,4}$ 6	$5_{1,5}$ 5	63021.71	0.03
$4_{1,4}$ 4	$3_{1,3}$ 3	12247.978	−0.002	$6_{2,5}$ 5,7	$5_{1,4}$ 4,6	61143.82	−0.02
$4_{1,4}$ 3	$3_{1,3}$ 2	12248.057	−0.025	$6_{2,5}$ 6	$5_{1,4}$ 5	61144.06	−0.02
$4_{1,4}$ 5	$3_{1,3}$ 4	12248.138	0.002	$7_{2,5}$ 6,8	$6_{1,6}$ 5,7	66552.30	0.00
$4_{1,4}$ 3	$3_{1,3}$ 3	12249.433	−0.009	$7_{2,5}$ 7	$6_{1,6}$ 6	66552.53	−0.02
$4_{1,3}$ 4	$3_{1,2}$ 3	12734.359	0.015	$7_{2,6}$	$6_{1,5}$	63902.50	−0.06
$4_{1,3}$ 3	$3_{1,2}$ 3	12735.751	0.027	$8_{2,6}$ 7,9	$7_{1,7}$ 6,8	70165.76	0.01
$4_{2,3}$ 5	$3_{2,2}$ 4	12492.343	−0.020	$8_{2,6}$ 8	$7_{1,7}$ 7	70165.95	−0.01
$4_{2,3}$ 3	$3_{2,2}$ 2	12492.473	−0.026	$8_{2,7}$	$7_{1,6}$	66600.98	−0.03
$4_{2,3}$ 4	$3_{2,2}$ 3	12491.798	−0.033	$9_{2,7}$	$8_{1,8}$	73867.97	0.00
$4_{2,2}$ 4	$3_{2,1}$ 4	12499.493	−0.016	$9_{2,8}$	$8_{1,7}$	69239.74	0.06
$4_{2,2}$ 5	$3_{2,1}$ 4	12500.001	−0.038	$10_{2,8}$	$9_{1,9}$	77665.64	−0.04
$4_{2,2}$ 3	$3_{2,1}$ 2	12500.187	0.011	$10_{2,9}$	$9_{1,8}$	71819.14	0.06
$5_{0,5}$ 6	$4_{0,4}$ 5	15600.641	0.022	$11_{2,10}$	$10_{1,9}$	74339.87	0.01
$5_{0,5}$ 4	$4_{0,4}$ 4	15602.195	−0.031	$12_{2,11}$	$11_{1,10}$	76802.82	0.04
$5_{1,5}$ 4,6	$4_{1,4}$ 3,5	15308.669	0.009	$19_{1,18}$	$18_{1,17}$	60242.00	0.03
$5_{1,4}$ 4,5,6	$4_{1,3}$ 3,4,5	15916.550	0.004	$19_{2,17}$	$18_{2,16}$	59974.44	0.03
$1_{1,0}$ 1	$1_{0,1}$ 0	14498.514	0.002	$20_{0,20}$	$19_{0,19}$	61565.11	−0.02
$1_{1,0}$ 2	$1_{0,1}$ 2	14499.654	0.000	$20_{1,20}$	$19_{1,19}$	61026.70	0.02
$1_{1,0}$ 0	$1_{0,1}$ 1	14499.900	−0.004	$20_{2,19}$	$19_{2,18}$	62292.35	−0.06

Downloaded from https://academic.oup.com/mnras/article/546/1/staf2224/8384188 by guest on 06 March 2026

Table A2. Measured rotational transition frequencies and corresponding deviations from the model of the ^{13}C1 isotopologue of TC conformer of 4-oxobutanenitrile.

$J'_{K'_a,K'_c}$ F'	$J''_{K''_a,K''_c}$ F''	Freq. (MHz)	o.-c. (MHz)
1 $_{0,1}$ 1	0 $_{0,0}$ 1	3086.854	0.007
1 $_{0,1}$ 2	0 $_{0,0}$ 1	3088.023	0.004
1 $_{0,1}$ 0	0 $_{0,0}$ 1	3089.782	0.005
1 $_{1,1}$ 2	0 $_{0,0}$ 1	17366.338	−0.002
1 $_{1,0}$ 1	1 $_{0,1}$ 0	14397.141	−0.004
1 $_{1,0}$ 2	1 $_{0,1}$ 2	14398.277	0.001
1 $_{1,0}$ 0	1 $_{0,1}$ 1	14398.509	0.001
1 $_{1,0}$ 1	1 $_{0,1}$ 2	14398.895	−0.007
1 $_{1,0}$ 2	1 $_{0,1}$ 1	14399.441	−0.006
1 $_{1,0}$ 1	1 $_{0,1}$ 1	14400.075	0.002
2 $_{0,2}$ 2	1 $_{0,1}$ 2	6173.730	0.008
2 $_{0,2}$ 1	1 $_{0,1}$ 0	6173.925	0.007
2 $_{0,2}$ 2	1 $_{0,1}$ 1	6174.898	0.004
2 $_{0,2}$ 3	1 $_{0,1}$ 2	6174.983	0.005
2 $_{1,2}$ 3	1 $_{1,1}$ 2	6055.928	0.009
2 $_{1,1}$ 1	2 $_{0,2}$ 1	14518.777	0.003
2 $_{1,1}$ 3	2 $_{0,2}$ 3	14519.149	0.001
2 $_{1,1}$ 2	2 $_{0,2}$ 2	14519.830	0.011
3 $_{0,3}$ 2	2 $_{0,2}$ 1	9260.263	−0.001
3 $_{0,3}$ 4	2 $_{0,2}$ 3	9260.519	0.013
3 $_{1,3}$ 3	2 $_{1,2}$ 2	9082.805	0.000
3 $_{1,3}$ 2,4	2 $_{1,2}$ 1,3	9083.175	0.027
3 $_{1,2}$ 2	2 $_{1,1}$ 1	9443.072	0.016
4 $_{0,4}$ 3,4,5	3 $_{0,3}$ 2,3,4	12343.727	−0.023
5 $_{0,5}$ 4,5,6	4 $_{0,4}$ 3,4,5	15424.031	−0.031

Table A3. Measured rotational transition frequencies and corresponding deviations from the model of the ^{13}C2 isotopologue of TC conformer of 4-oxobutanenitrile.

$J'_{K'_a,K'_c}$ F'	$J''_{K''_a,K''_c}$ F''	Freq. (MHz)	o.-c. (MHz)
1 $_{0,1}$ 1	0 $_{0,0}$ 1	3117.900	0.002
1 $_{0,1}$ 2	0 $_{0,0}$ 1	3119.072	0.004
1 $_{0,1}$ 0	0 $_{0,0}$ 1	3120.828	0.005
1 $_{1,1}$ 2	0 $_{0,0}$ 1	17196.779	−0.003
1 $_{1,1}$ 1	0 $_{0,0}$ 1	17197.332	−0.007
1 $_{1,0}$ 1	1 $_{0,1}$ 0	14200.748	0.004
1 $_{1,0}$ 2	1 $_{0,1}$ 2	14201.905	0.019
1 $_{1,0}$ 1	1 $_{0,1}$ 2	14202.489	−0.010
2 $_{0,2}$ 2	1 $_{0,1}$ 2	6235.758	0.000
2 $_{0,2}$ 1	1 $_{0,1}$ 0	6235.954	0.001
2 $_{0,2}$ 2	1 $_{0,1}$ 1	6236.927	0.000
2 $_{0,2}$ 3	1 $_{0,1}$ 2	6237.013	0.002
2 $_{0,2}$ 1	1 $_{0,1}$ 1	6238.874	−0.004
2 $_{1,2}$ 3	1 $_{1,1}$ 2	6113.813	0.010
2 $_{1,1}$ 3	2 $_{0,2}$ 3	14327.034	−0.003
2 $_{1,1}$ 2	2 $_{0,2}$ 2	14327.694	0.001
3 $_{0,3}$ 3	2 $_{0,2}$ 3	9352.083	−0.010
3 $_{0,3}$ 2	2 $_{0,2}$ 1	9353.144	−0.008
3 $_{0,3}$ 4	2 $_{0,2}$ 3	9353.403	0.009
3 $_{0,3}$ 2	2 $_{0,2}$ 3	9353.844	−0.005
3 $_{1,3}$ 2,4	2 $_{1,2}$ 1,3	9169.938	0.0024
3 $_{1,2}$ 2,4	2 $_{1,1}$ 1,3	9542.487	0.0070
4 $_{0,4}$ 3,4,5	3 $_{0,3}$ 2,3,4	12467.297	0.0008

Table A4. Measured rotational transition frequencies and corresponding deviations from the model of the ^{13}C3 isotopologue of TC conformer of 4-oxobutanenitrile.

$J'_{K'_a,K'_c}$ F'	$J''_{K''_a,K''_c}$ F''	Freq. (MHz)	o.-c. (MHz)
1 $_{0,1}$ 1	0 $_{0,0}$ 1	3119.657	−0.001
1 $_{0,1}$ 2	0 $_{0,0}$ 1	3120.828	0.001
1 $_{0,1}$ 0	0 $_{0,0}$ 1	3122.577	−0.003
1 $_{1,1}$ 1	0 $_{0,0}$ 1	17377.215	0.004
1 $_{1,0}$ 1	1 $_{0,1}$ 0	14377.229	−0.004
1 $_{1,0}$ 2	1 $_{0,1}$ 2	14378.369	−0.003
1 $_{1,0}$ 1	1 $_{0,1}$ 2	14378.993	0.007
1 $_{1,0}$ 2	1 $_{0,1}$ 1	14379.530	−0.011
1 $_{1,0}$ 1	1 $_{0,1}$ 1	14380.154	−0.001
2 $_{0,2}$ 2	1 $_{0,1}$ 2	6239.302	−0.007
2 $_{0,2}$ 1	1 $_{0,1}$ 0	6239.507	0.004
2 $_{0,2}$ 2	1 $_{0,1}$ 1	6240.477	0.000
2 $_{0,2}$ 3	1 $_{0,1}$ 2	6240.563	0.002
2 $_{0,2}$ 1	1 $_{0,1}$ 1	6242.428	0.003
2 $_{1,2}$ 2	1 $_{1,1}$ 1	6117.760	0.022
2 $_{1,2}$ 3	1 $_{1,1}$ 2	6118.949	−0.001
2 $_{1,1}$ 3	2 $_{0,2}$ 3	14501.870	0.008
3 $_{0,3}$ 3	2 $_{0,2}$ 3	9357.485	−0.012
3 $_{0,3}$ 2	2 $_{0,2}$ 1	9358.540	−0.015
3 $_{0,3}$ 4	2 $_{0,2}$ 3	9358.803	0.007
3 $_{1,3}$ 3	2 $_{1,2}$ 2	9177.338	0.004
3 $_{1,3}$ 2,4	2 $_{1,2}$ 1,3	9177.669	−0.007
3 $_{1,2}$ 2,4	2 $_{1,1}$ 1,3	9545.342	0.008

Table A5. Measured rotational transition frequencies and corresponding deviations from the model of the ^{13}C4 isotopologue of TC conformer of 4-oxobutanenitrile.

$J'_{K'_a,K'_c}$ F'	$J''_{K''_a,K''_c}$ F''	Freq. (MHz)	o.-c. (MHz)
1 $_{0,1}$ 1	0 $_{0,0}$ 1	3089.956	0.005
1 $_{0,1}$ 2	0 $_{0,0}$ 1	3091.122	0.004
1 $_{0,1}$ 0	0 $_{0,0}$ 1	3092.870	−0.001
1 $_{1,1}$ 2	0 $_{0,0}$ 1	17467.348	−0.001
1 $_{1,1}$ 1	0 $_{0,0}$ 1	17467.913	0.012
1 $_{1,0}$ 1	1 $_{0,1}$ 0	14494.372	0.006
1 $_{1,0}$ 2	1 $_{0,1}$ 2	14495.506	0.004
1 $_{1,0}$ 0	1 $_{0,1}$ 1	14495.742	−0.006
1 $_{1,0}$ 1	1 $_{0,1}$ 2	14496.110	−0.008
2 $_{0,2}$ 1	1 $_{0,1}$ 0	6180.140	0.005
2 $_{0,2}$ 2	1 $_{0,1}$ 1	6181.116	0.008
2 $_{0,2}$ 3	1 $_{0,1}$ 2	6181.199	0.007
2 $_{0,2}$ 1	1 $_{0,1}$ 1	6183.063	0.008
2 $_{1,1}$ 1	2 $_{0,2}$ 1	14615.309	−0.001
2 $_{1,1}$ 3	2 $_{0,2}$ 3	14615.671	−0.005
2 $_{1,1}$ 2	2 $_{0,2}$ 2	14616.335	0.000
3 $_{0,3}$ 2	2 $_{0,2}$ 1	9269.619	−0.001
3 $_{0,3}$ 3	2 $_{0,2}$ 2	9269.802	−0.012
3 $_{0,3}$ 4	2 $_{0,2}$ 3	9269.878	0.017
3 $_{1,2}$ 3	2 $_{1,1}$ 2	9450.997	0.008
3 $_{1,2}$ 2,4	2 $_{1,1}$ 1,3	9451.335	0.000
4 $_{0,4}$ 3	3 $_{0,3}$ 2	12356.203	−0.018
4 $_{0,4}$ 5	3 $_{0,3}$ 4	12356.324	−0.010

Downloaded from https://academic.oup.com/mnras/article/546/1/staf2224/8384188 by guest on 06 March 2026

Table A6. Measured rotational transition frequencies and corresponding deviations from the model of the ^{18}O isotopologue of TC conformer of 4-oxobutanenitrile.

$J'_{K'_a,K'_c}$ F'	$J''_{K''_a,K''_c}$ F''	Freq. (MHz)	o.-c. (MHz)
$1_{1,1}$ 2	$0_{0,0}$ 1	17087.181	0.000
$2_{0,2}$ 1	$1_{0,1}$ 0	6032.992	0.003
$2_{0,2}$ 2	$1_{0,1}$ 1	6033.979	0.004
$2_{0,2}$ 3	$1_{0,1}$ 2	6034.071	0.011
$2_{0,2}$ 1	$1_{0,1}$ 1	6035.949	0.001
$3_{0,3}$ 4	$2_{0,2}$ 3	9049.217	−0.013
$3_{1,3}$ 2,4	$2_{1,2}$ 1,3	8878.004	0.000

Table A7. Measured rotational transition frequencies and corresponding deviations from the model of the ^{15}N isotopologue of TC conformer of 4-oxobutanenitrile.

$J'_{K'_a,K'_c}$	$J''_{K''_a,K''_c}$	Freq. (MHz)	o.-c. (MHz)
$1_{0,1}$	$0_{0,0}$	3041.633	0.003
$1_{1,1}$	$0_{0,0}$	17461.238	0.018
$1_{1,0}$	$1_{0,1}$	14534.928	−0.008
$2_{0,2}$	$1_{0,1}$	6082.579	0.008
$2_{1,1}$	$2_{0,2}$	14650.961	−0.010
$3_{0,3}$	$2_{0,2}$	9122.134	0.001
$3_{1,2}$	$2_{1,1}$	9297.493	0.017
$4_{0,4}$	$3_{0,3}$	12159.606	−0.023

Table A8. Experimental spectroscopic parameters of the ^{13}C, ^{15}N, and ^{18}O isotopologues of the TC conformer of 4-oxobutanenitrile, derived from the fit of its rotational transitions recorded in the 2−18 GHz range.

Parameter	^{13}C1	^{13}C2	^{13}C3
A_0 (MHz)	15882.5029(43)	15699.5295(27)	15877.7092(32)
B_0 (MHz)	1603.8960(20)	1621.5271(10)	1621.5922(15)
C_0 (MHz)	1483.9275(17)	1497.3456(10)	1499.0399(12)
$\frac{3}{2}\chi_{aa}$ (MHz)	−5.859(19)	−5.8499(98)	−5.843(11)
$\frac{1}{4}(\chi_{bb}-\chi_{cc})$ (MHz)	−0.0676(75)	−0.0461(70)	−0.0504(79)
N	25	24	23
σ (kHz)	11	7	8
Parameter	^{13}C4	^{18}O	^{15}N
A_0 (MHz)	15981.6204(32)	15636.5033(73)	15998.0781(83)
B_0 (MHz)	1605.1034(13)	1566.5668(32)	1578.4878(32)
C_0 (MHz)	1485.8203(15)	1450.7766(24)	1463.1422(36)
$\frac{3}{2}\chi_{aa}$ (MHz)	−5.840(13)	−5.918(19)	...
$\frac{1}{4}(\chi_{bb}-\chi_{cc})$ (MHz)	−0.0520(54)	[0][a]	...
N	23	7	8
σ (kHz)	8	7	13

[a] Fixed to zero in the fit.

This paper has been typeset from a TEX/LATEX file prepared by the author.

Downloaded from https://academic.oup.com/mnras/article/546/1/staf2224/8384188 by guest on 06 March 2026

© The Author(s) 2025.
Published by Oxford University Press on behalf of Royal Astronomical Society. This is an Open Access article distributed under the terms of the Creative Commons Attribution License (https://creativecommons.org/licenses/by/4.0/), which permits unrestricted reuse, distribution, and reproduction in any medium, provided the original work is properly cited.